Modeling Nonlinear Steady-State Induction Heating Processes

K. Roppert, F. Toth, and M. Kaltenbacher

Institute for Mechanics and Mechatronics, Vienna University of Technology (TU Wien), 1040 Vienna, Austria

In this article, an efficient simulation strategy for a fully coupled nonlinear magnetic–thermal problem is presented. The solution-dependent magnetic subproblem is solved with a harmonic balancing scheme, with the main focus on the correct choice of the material model (magnetization curve). To further increase the computational efficiency, a non-conforming interface approach is used, based on the jump operators and penalty terms. This method drastically decreases the meshing time because different mesh sizes can be combined without taking care of element distortions in transition layers between fine and coarse parts of the mesh.

Index Terms—**Eddy currents, electromagnetic induction, finite-element analysis, Maxwell equations.**

I. Introduction

MAGNETIC–THERMAL problems arise in a wide range of possible applications, e.g., induction heating or thermal analysis of transformers or motors. In this article, we focus on the efficient simulation of induction heating processes for thin steel sheets, where the inductors are made of massive conductive material, and therefore, eddy currents inside the inductor have to be taken into account by means of global excitation (total current or voltage).

The classical way would be to consider the full $\boldsymbol{A}-V$ or $\boldsymbol{T}-\Phi$ formulation with additional constraint equations to define the voltage or total current through an electric port [10]. We, on the other hand, use a modified version based on the work of [6], [8], [9], which enables the decoupling of equations for $\boldsymbol{A}$ and V and significantly improves the performance by introducing a precomputation step for V.

Although there exist methods improving the efficiency of magnetic–thermal simulations in the time domain, see [2], we consider the nonlinear eddy-current problem solely in the frequency domain and use the multiharmonic ansatz approach from [4], together with an alternating time–frequency scheme [3] to obtain correct reluctivity values in the respective harmonics.

Since these induction heating applications involve setups, where a finely meshed, structured region (the sheet) must be combined with a more complexly shaped (depending on the inductor winding geometry) air domain, we present a methodology for nonconforming interfaces in $H(\mathrm{curl},\Omega)$ function space, based on the Nitsche's idea [7] for the time-harmonic eddy-current problem in $\boldsymbol{A}$, which also holds for the modified $\boldsymbol{A}-V$ formulation with some minor assumptions.

II. Eddy-Current Problem

The considered eddy-current problem in its time domain form

$$\nabla\times\nu(||\nabla\times\boldsymbol{A}||)\,\nabla\times\boldsymbol{A}=\boldsymbol{J}_{\mathrm{i}}-\gamma(T)\frac{\partial\boldsymbol{A}}{\partial t} \tag{1}$$

Manuscript received July 14, 2019; revised October 25, 2019 and November 15, 2019; accepted November 28, 2019. Date of publication January 14, 2020; date of current version February 19, 2020. Corresponding author: K. Roppert (e-mail: klaus.roppert@tuwien.ac.at).

Color versions of one or more of the figures in this article are available online at http://ieeexplore.ieee.org.

Digital Object Identifier 10.1109/TMAG.2019.2957343

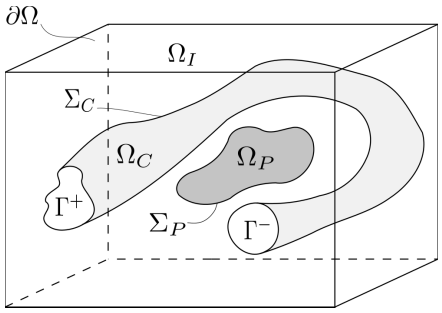

Fig. 1. Considered setup of inductor, air, and conducting passive part.

is solved for the magnetic vector potential $\boldsymbol{A}$, where $\nu(||\nabla\times\mathbf{A}||)$ represents the solution-dependent reluctivity, based on the commutation curve, $\boldsymbol{J}_{\mathrm{i}}$ is the impressed current density, and $\gamma(T)$ is the temperature-dependent electric conductivity.

A. Excitation With Global Quantities

Let us consider the domain, depicted in Fig. 1, with Ω_C as the conducting ($\gamma>0$) inductor, Ω_P the passive conductive part, Ω_I the surrounding air ($\gamma=0$), and Γ^+, Γ^- as the electric ports of the inductor. The boundary of the whole domain is denoted as $\partial\Omega=\partial\Omega_I\cup\Gamma^+\cup\Gamma^-$. Together with the definition of the appropriate function space $W_h\subset H_0(\nabla\times,\Omega):=\{\boldsymbol{a}\in H(\mathrm{curl},\Omega)\,|\,\boldsymbol{n}\times\boldsymbol{a}=0,\ \text{on}\ \partial\Omega$ and $V_h\subset H^1(\Omega)$, we can define the classical weak form of $\boldsymbol{A}-V$ formulation as follows. Find $\boldsymbol{A}\in W_h$ and $V\in V_h$ such that

$$\begin{aligned}&(\nu\nabla\times\boldsymbol{A},\nabla\times\boldsymbol{A}')_\Omega+j\omega(\gamma\boldsymbol{A},\boldsymbol{A}')_\Omega+(\gamma\nabla V,\boldsymbol{A}')_\Omega=0\\&j\omega(\boldsymbol{A},\nabla\boldsymbol{V}')_\Omega+(\gamma\nabla V,\nabla V')_\Omega=0\\&\forall\boldsymbol{A}'\in W_h,\quad V'\in V_h\end{aligned} \tag{2}$$

where $(\cdot,\cdot)_\Omega$ denotes a volume integral with a dot product between its arguments over domain Ω. The magnetic boundary conditions (BCs) are $\boldsymbol{A}\times\boldsymbol{n}=0$ on $\partial\Omega$ and electric BCs $\boldsymbol{n}\times\boldsymbol{E}=\boldsymbol{n}\times(-\nabla V-\partial\boldsymbol{A}/\partial t)=0$ on Γ^+,Γ^-, which can be split into two parts

$$\boldsymbol{n}\times\nabla V=0\ \text{and}\ \boldsymbol{n}\times\partial\boldsymbol{A}/\partial t=0 \tag{3}$$

where the first condition is satisfied for $V=$ const., and the second one is already incorporated through the

magnetic BC. A voltage excitation, with voltage U, in the $\boldsymbol{A}-V$ formulation (2) can now be accomplished by defining the following BCs for the electric scalar potential:

$$V_{|\Gamma^+} = U, \quad V_{|\Gamma^+} = 0. \tag{4}$$

In [6], it is shown that the solution of (2) is independent of V inside Ω_C, as long as the BCs (4) are fulfilled, which means that we can define an arbitrary $H^1(\Omega)$ extension of V, denoted as $\tilde{V}$. Since edge elements are used for the discretized space $W_h \subset H(\text{curl}, \Omega)$ and nodal elements for $V_h \subset H^1(\Omega)$, we can use the findings of [8] and [9] to decouple the computation of $\boldsymbol{A}$ and $\tilde{V}$. The computation of $\tilde{V} = U\tilde{V}_0$, with unit source BCs $\tilde{V}_{0|_{\Gamma^+}} = 1$ and $\tilde{V}_{0|_{\Gamma^-}} = 0$, can either be accomplished by defining a transition layer, e.g., in [9] or by solving the electrokinetic problem

$$\left(\gamma \nabla \tilde{V}_0, \nabla \tilde{V}_0'\right)_{\Omega_C} = 0 \quad \forall \tilde{V}_0' \in V_h. \tag{5}$$

After this precompute step, an excitation with global voltage U at the electric ports can be defined as follows. Find $\boldsymbol{A} \in W_h$ such that for all $\boldsymbol{A}' \in W_h$ there holds

$$(\nabla\times\boldsymbol{A}, \nu\nabla\times\boldsymbol{A}')_\Omega + j\omega\gamma\,(\boldsymbol{A}, \boldsymbol{A}')_\Omega + U(\gamma\,\nabla\tilde{V}_0, \boldsymbol{A}')_\Omega = 0. \tag{6}$$

One can see that prescribing U is a strong constraint because the value is directly prescribed, which is the equivalent to Dirichlet BC in a spatial domain. Showing the vanishing divergence of the current density $\boldsymbol{J} = -\gamma\,(j\omega\boldsymbol{A} + U\nabla\tilde{V}_0)$ can be done by investigating the two contributions separately. Since we are using edge elements, the divergence of the first term is zero because $H(\text{curl}, \Omega)$ is the kernel of the divergence operator, and the second term vanishes because $\tilde{V}_0$ solves the homogeneous Laplace equation (5), and therefore, $\nabla\cdot\nabla\tilde{V}_0 = 0$.

For prescribing a total current excitation, we need to constrain the total current through the electric ports (multiplication with $\tilde{V}_0$ in (7) is valid, since it is one at Γ^+ and helps us to use the divergence theorem in the next step). By using $\boldsymbol{J}\cdot\boldsymbol{n} = 0$ on Σ_C and $\nabla\cdot\boldsymbol{J} = 0$ in Ω_C, we can use the divergence theorem to obtain the constraint equation, enforcing the total current in a weak sense

$$\begin{aligned} I &= -\int_{\Gamma^+} \tilde{V}_0 \boldsymbol{J}\cdot\boldsymbol{n} = -\int_{\partial\Omega_C} \tilde{V}_0 \boldsymbol{J}\cdot\boldsymbol{n} \\ &= -\int_{\Omega_C} \boldsymbol{J}\cdot\nabla\tilde{V}_0 = \int_{\Omega_C} \gamma\,(j\omega\boldsymbol{A} + U\nabla\tilde{V}_0)\cdot\nabla\tilde{V}_0. \end{aligned} \tag{7}$$

Finally, we can write the weak form for total current excitation as follows. Find $\boldsymbol{A} \in W_h$ and $U \in C^1$ such that for all $\boldsymbol{A}' \in W_h$ there holds

$$\begin{aligned} (\nabla\times\boldsymbol{A}, \nu\nabla\times\boldsymbol{A}')_\Omega + j\omega\gamma\,(\boldsymbol{A}, \boldsymbol{A}')_\Omega + U(\gamma\,\nabla\tilde{V}_0, \boldsymbol{A}')_\Omega &= 0 \\ (\gamma\, j\omega\boldsymbol{A}, \nabla\tilde{V}_0)_{\Omega_C} + U(\nabla\tilde{V}_0, \nabla\tilde{V}_0)_{\Omega_C} &= I. \end{aligned} \tag{8}$$

B. Nonconforming Nitsche Interfaces

A substantial performance improvement can be achieved by using nonconforming Nitsche interfaces for 3-D edge elements in $H(\text{curl}, \Omega)$. Assume a set up of two independently meshed domains $\overline{\Omega}_1$, $\overline{\Omega}_2$ with their common interface $\Gamma_I = (\overline{\Omega}_1 \setminus \Omega_1) \cap (\overline{\Omega}_2 \setminus \Omega_2)$, as depicted in Fig. 2.

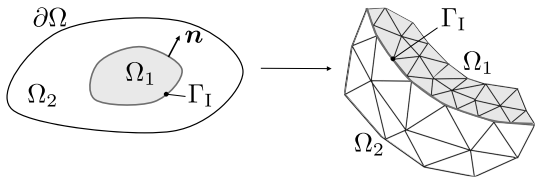

Fig. 2. Computational domain with two subregions Ω_1 and Ω_2 with different discretizations.

This approach is based on the Nitsche's idea [7] to incorporate Dirichlet boundary conditions into the weak form, which is also the main idea of discontinuous Galerkin (DG) finite-element methods. Let us now consider the domain setup from Fig. 2, where the discretization $\mathcal{T}_h^1$ of Ω_1 and $\mathcal{T}_h^2$ of Ω_2, with $\mathcal{T}_h = \mathcal{T}_h^1 \cup \mathcal{T}_h^2$ conforms to their interior but non-conforming across their common interface Γ_I. The global set of facets is now split into purely interior facets $\mathcal{F}_h^i$, interface facets $\mathcal{F}_h^I$, and essential facets (Dirichlet boundary) $\mathcal{F}_h^e$. By considering the full DG formulation of (1), eliminating jumps across $\mathcal{F}_h^i$ and neglecting the direct prescription of Dirichlet BC (for better readability), we obtain the following weak form where the DG terms only remain on the non-conforming interface facets $\mathcal{F}_h^I$. Find $\boldsymbol{A} \in W_h$ such that $\forall \boldsymbol{A}' \in W_h$

$$\begin{aligned} &(\nu\nabla\times\boldsymbol{A}, \nabla\times\boldsymbol{A}')_{\Omega_{1,2}} + (j\omega\gamma\,\boldsymbol{A}, \boldsymbol{A}')_{\Omega_{1,2}} \\ &\quad - \sum_{F\in\mathcal{F}_h^I} \langle 2(\nu_1\nabla\times\boldsymbol{A}_1\times\boldsymbol{n}), [\boldsymbol{A}']\rangle_F \\ &\quad - \sum_{F\in\mathcal{F}_h^I} \langle 2\,\epsilon(\nu_1\nabla\times\boldsymbol{A}_1'\times\boldsymbol{n}), [\boldsymbol{A}]\rangle_F \\ &\quad + \beta \sum_{F\in\mathcal{F}_h^I} \left\langle \frac{\overline{\nu}\,p_E^2}{h_E}[\boldsymbol{n}\times\boldsymbol{A}], [\boldsymbol{n}\times\boldsymbol{A}'] \right\rangle_F = (\boldsymbol{J}_i, \boldsymbol{A}')_\Omega \end{aligned} \tag{9}$$

where $\langle\cdot,\cdot\rangle_F$ denote integrals over surface F with a dot product between its arguments, ν_1 is the reluctivity on the interface side of Ω_1, $\overline{\nu}$ is the averaged reluctivity of both sides on the interface, p_E is the element order, h_E is the local length scale of the element, and β is the penalization parameter. According to [7], this Nitsche- (penalization-) parameter has to be chosen "large enough" in order to ensure convergence. On the other hand, the higher this parameter is chosen, the more ill conditioned the resulting system matrix is and when reaching a certain limit, and the solution seems to suffer from numerical instabilities, observed in Section IV.

This methodology for the classical $\boldsymbol{A}$ formulation can also be expanded to the $\boldsymbol{A}-\tilde{V}_0$ global excitation formulations (6) and (8) with the only restriction that the inductor is not touching any conducting part ($\Omega_C \cap \Omega_P = \emptyset$) and the interface is either located completely in the air domain or at Σ_C or Σ_P but not inside the inductor.

C. Harmonic Balance FEM

In order to solve (1) in the frequency domain, while retaining its nonlinearity, we expand $\boldsymbol{A}$, $\nu(||\nabla\times\boldsymbol{A}||)$ and the excitation quantity with the multiharmonic ansatz into the

truncated Fourier series

$$\boldsymbol{f}(\boldsymbol{x},t)=\sum_{k=-N}^{N}\hat{\boldsymbol{f}}_k(\boldsymbol{x})\cdot e^{jk\omega t},\quad \text{with}\ \ \hat{\boldsymbol{f}}_{-k}=\hat{\boldsymbol{f}}_k^{*}. \tag{10}$$

The efficient solution strategy to solve the large systems is based on [4]. An important aspect is the correct evaluation of the reluctivity Fourier coefficient $\hat{\nu}_k$, where an alternating time–frequency scheme (harmonic balancing) is applied, together with the anhysteretic curve [5] as the model for the nonlinear reluctivity. Using the anhysteretic instead of the classical commutation curve increases the convergence significantly because the latter one has an unphysical flattening at small field strengths when considering the cycle on the hysteresis curve (Rayleigh region).

III. Thermal Problem

The thermal field is simulated with a nonlinear convection diffusion equation

$$\frac{\partial \rho c(T)T}{\partial t}-\nabla\cdot(\lambda(T)\nabla T-\rho c(T)T\boldsymbol{u}(t))=\dot{q} \tag{11}$$

where $c(T)$ represents the temperature-dependent specific heat capacity, $\lambda(T)$ is the heat conduction coefficient, T is the temperature, and $\boldsymbol{u}$ is the velocity. The volumetric heat source term $\dot{q}$ is represented by the Joule losses

$$\dot{q}=\boldsymbol{E}\cdot\boldsymbol{J} \tag{12}$$

with the electric-field intensity $\boldsymbol{E}=-\partial\boldsymbol{A}/\partial t$, respectively, $\boldsymbol{E}=-\partial\boldsymbol{A}/\partial t-U\nabla\tilde{V}_0$ for the global excitation formulation. Due to the large time scale differences between the magnetic and thermal fields, we can justify to consider the heat source $\dot{q}(t)$ as time independent, i.e., averaging $\dot{q}(t)$ over one period of the base excitation frequency. Therewith the flexibility to consider the nonlinear thermal problem in time as well as in steady-state domain is obtained.

IV. Numerical Examples

In the following, two numerical examples are presented, highlighting the importance and benefits of the methods, presented above. The inductor is made of copper with electric conductivity $5\cdot10^7$ S/m and relative reluctivity $\nu_r=1$. For the sheet, an electric conductivity of $9.17431\cdot10^5$ S/m is used and a measured anhysteretic curve with linear relative reluctivity of 0.03 and saturation flux density of 1.6 T. In Fig. 3, the general dimensions of the setup are given.

A. 2-D Model

The first numerical experiment is to compare the Joule losses in the sheet between a model with Nitsche interfaces between the sheet and air domain and a conformlly meshed model. In this setup, the conductivity and the reluctivity are discontinuous across the interface, and the influence of the penalization parameter on the Joule losses is investigated.

In Fig. 4, the effect of the Nitsche- (penalization-) parameter is investigated, and we observe the expected behavior discussed above, where the error is decreasing up to a certain threshold of the parameter and then suffers from numerical instabilities. Based on Fig. 4 and other parameter studies, we can conclude that choosing the Nitsche parameter in the range between 100 and 1500 seems to be a good choice for many applications in 2-D as well as 3-D, with a similar setup as depicted in Fig. 3.

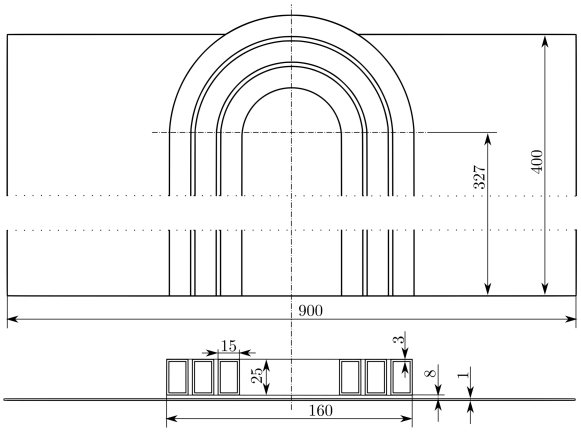

Fig. 3. 3-D half model and 2-D setup with dimensions in millimeters.

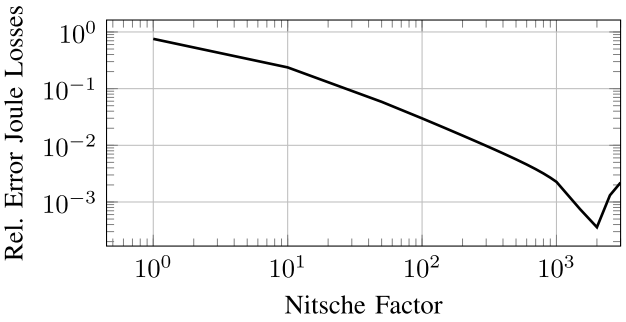

Fig. 4. Relative error between Joule losses with NC Nitsche interface and conforming mesh with the fixed mesh size.

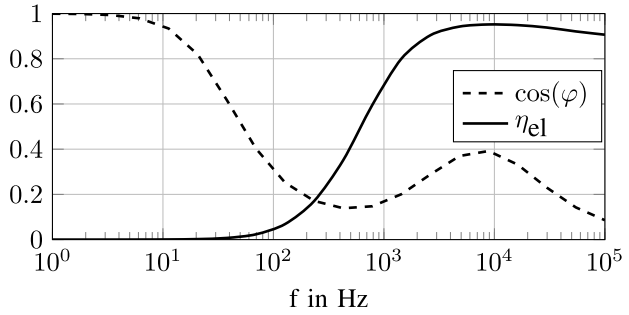

Fig. 5. Phase shift $\cos(\varphi)$ between global voltage and current and electrical efficiency η_{el} depending on the excitation frequency.

Since an excitation with global quantities is used, the phase shift between total current and voltage can be evaluated and an optimal working point in terms of electrical efficiency can be observed, which is depicted in Fig. 5.

In order to investigate the influence of the nonlinear reluctivity on the temperature field, three different multiharmonic simulations with different numbers of considered harmonics in the multiharmonic ansatz (10) were carried out and compared

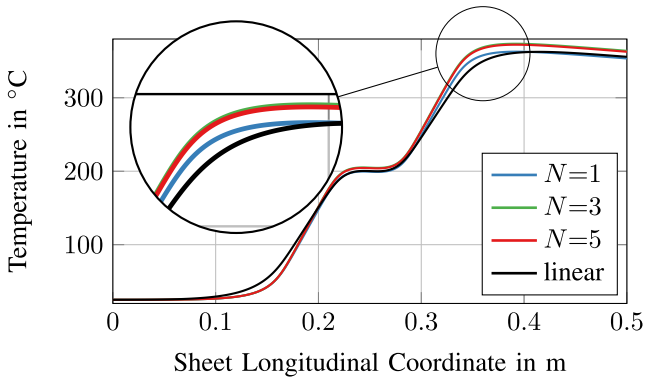

Fig. 6. Comparison of harmonic balancing solution with different numbers of considered harmonics.

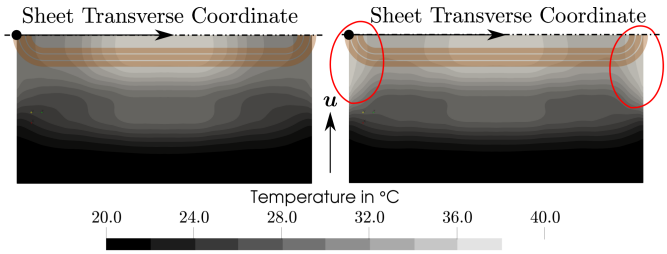

Fig. 7. Sheet temperature for impressed current (left) and global current excitation (right), with more physical edge overheating (highlighted in red).

to a linear harmonic simulation (see Fig. 6). In general, the nonlinearity has minor influence on the temperature, which is a particularity of transverse flux induction heating devices, even when the flux density in the sheet reaches far into saturation, which is the case in this example.

B. 3-D Model

A characteristic of transverse flux induction heating devices, as depicted in Fig. 3, is that it is difficult to obtain a homogeneous temperature distribution across the sheets transverse coordinate, due to edge effects, caused by the inductor head.

In particular, for 3-D simulations with close multi-turn inductors, it is essential to use global excitation because skin and proximity effects significantly change the resulting magnetic field and, therefore, also the temperature of the sheet, which can be seen in Fig. 7. At the outer edges of the sheet (beneath the inductor head), a distinct overheating can be observed, depicted in Fig. 8, which is common for this kind of induction heating devices but only occurs for the simulation with global excitation, due to the eddy-current distribution.

Also for the 3-D simulation, non-conforming interfaces, based on (9), were used, where the sheet is meshed with the structured hexahedral (hex) elements and the air domain with tetrahedrons (tet). For this combination, the penalization parameter in (9) has to be chosen slightly higher than that for hex–hex or tet–tet interfaces; in our case, it was set to 2600.

Plotting the temperature across the transverse direction of the sheet, the different temperature behavior, especially at the edges, becomes even more evident, depicted in Fig. 8.

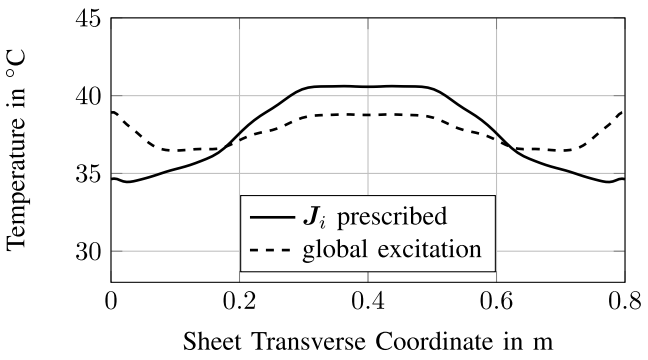

Fig. 8. Sheet temperature along the transverse coordinate from Fig. 7, at the downstream edge.

V. Conclusion

A specialized $\boldsymbol{A} - V$ formulation for excitation with global electric quantities was presented, which decouples the computation of $\boldsymbol{A}$ and V when using edge and nodal elements respectively. This increases the computational performance, compared to the classical $\boldsymbol{A} - V$ formulation because the electric scalar potential can be precomputed by solving a Laplace equation (electrokinetic problem), which is straightforward and can be highly parallelized and the system for $\boldsymbol{A}$ is better conditioned. Furthermore, a non-conforming Nitsche interface formulation was presented for edge elements in H(curl), which helps to significantly decrease the preprocessing time (meshing) because no conforming transition layers between different element types or mesh sizes have to be constructed.

References

[1] C. Kaufmann *et al.*, "Efficient frequency-transient co-simulation of coupled heat-electromagnetic problems," *J. Math. Ind.*, vol. 4, no. 1, 2014, Art. no. 1.

[2] O. Biro and K. Preis, "An efficient time domain method for nonlinear periodic eddy current problems," *IEEE Trans. Magn.*, vol. 42, no. 4, pp. 695–698, Apr. 2006.

[3] S. Yamada, K. Bessho, and J. Lu, "Harmonic balance finite element method applied to nonlinear AC magnetic analysis," *IEEE Trans. Magn.*, vol. 25, no. 4, pp. 2971–2973, Jul. 1989.

[4] F. Bachinger, M. Kaltenbacher, and S. Reitzinger, "An efficient solution strategy for the HBFE method," in *Proc. IGTE*, 2002, pp. 385–389.

[5] D. Jiles, *Introduction to Magnetism and Magnetic Materials*, 3rd ed. Boca Raton, FL, USA: CRC Press, 2016.

[6] R. Hiptmair and O. Sterz, "Current and voltage excitations for the eddy current model," *Int. J. Numer. Model., Electron. Netw., Devices Fields*, vol. 18, no. 1, pp. 1–21, 2005.

[7] J. Nitsche, "Über ein Variationsprinzip zur Lösung von Dirichlet–Problemen bei Verwendung von Teilräumen, die keinen Randbedingungen unterworfen sind," *Abhandlungen Math. Seminar Univ. Hambur*, vol. 36, no. 1, pp. 9–15, 1971.

[8] P. Dular, W. Legros, and A. Nicolet, "Coupling of local and global quantities in various finite element formulations and its application to electrostatics, magnetostatics and magnetodynamics," *IEEE Trans. Magn.*, vol. 34, no. 5, pp. 3078–3081, Sep. 1998.

[9] P. Dular, F. Henrotte, and W. Legros, "A general and natural method to define circuit relations associated with magnetic vector potential formulations," *IEEE Trans. Magn.*, vol. 35, no. 3, pp. 1630–1633, May 1999.

[10] O. Bir, P. Bohm, K. Preis, and G. Wachutka, "Edge finite element analysis of transient skin effect problems," *IEEE Trans. Magn.*, vol. 36, no. 4, pp. 835–839, Jul. 2000.

[11] R. Casagrande, R. Hiptmair, and J. Ostrowski, "An *a priori* error estimate for interior penalty discretizations of the Curl-Curl operator on non-conforming meshes," *J. Math. Ind.*, vol. 6, no. 1, p. 4, 2016.